COMMUNICATION

Interface-Engineered Co_3O_4 Nano-Islands on Cu Substrate for High-Efficiency Electrocatalytic Nitrate-to-Ammonia Conversion

Received 00th January 20xx,
Accepted 00th January 20xx

DOI: 10.1039/x0xx00000x

Tong Xu[a,1], Zhenxiao Wang[a,1], Hongyang Zhu[a], Ziwei Zhang[a], Yangping Zhang[a,*], Danhong Shang[a], Linzhi Zhai[a], Tongyi Yang[a], Mengnan Wang[b,*], Fu Yang[a,*]

The core@shell C/Cu@Co_3O_4 catalyst with interfacial-engineered nano-islands on Cu substrate were constructed, featuring accelerated electron-transfer property and optimized nitrate trapping through the synergetic interfacial effect, achieving a remarkable NH_3 yield of 57.4±2.9 mg·h^{-1}·mg$_{cat}^{-1}$ and high Faraday efficiency of 98.4 ± 1.2%, surpassing most reported non-precious metal catalysts.

Ammonia plays a vital role as both a carbon-free energy carrier and a key precursor in fertilizer production[1, 2]. However, its industrial synthesis via the Haber-Bosch process is still a high-energy process under high temperature and pressure conditions[3, 4]. Electrocatalytic nitrogen reduction (NRR) emerges as a green and sustainable alternative for ammonia production, suffering from inherent limitations including the strong N≡N bond (941 kJ·mol^{-1}), low N_2 solubility and parasitic hydrogen evolution reaction (HER)[5-8]. In contrast, nitrate (NO_3^-) reduction reaction (NO_3^-RR) offers superior feasibility due to its lower dissociation energy (N=O, 204 kJ·mol^{-1}), high solubility, and dual environmental/energy benefits through wastewater remediation[9-11]. However, the NO_3^-RR involves a complex eight-electron transfer mechanism with multiple intermediates (e.g., *NO_2, *NO, *N), requiring finely tuned *N hydrogenation steps to suppress byproducts (e.g., N_2). This demands effective catalysts with optimized adsorption energetics to selectively promote NH_3 generation[12-14].

Copper-based catalysts have been widely investigated due to their affordability, moderate binding strength with NO_3^- and tunable d-band centers. Yet their catalytic performance is often limited by insufficient *H supply and intermediate accumulation (e.g., NO_2^-), compromising product selectivity[15, 16]. To overcome these issues, various structural and electronic modifications including alloying, heterostructure construction, defect engineering have been explored. For instance, Co-Cu bimetallic systems exhibit synergistic electronic modulation that lower *NO→*N barriers while porous carbon species enhance intermediate concentration and charge transfer[17-19]. Despite these advancements, achieving simultaneous high NH_3 yield greater than 2 mg·h^{-1}·cm^{-2} and near-unity Faradaic efficiency under mild conditions remains challenging necessitating innovative interface engineering strategies[20, 21].

Herein, we demonstrate a metal-organic framework (MOF)-mediated topological synthesis strategy to construct Cu-Co heterostructured catalysts featuring spatially confined Co nanoislands on a porous Cu substrate. The C/Cu@Co_3O_4 architecture is synthesized through sequential coordination of polydopamine (PDA) and cobalt ions on Cu-BTC frameworks, followed by controlled argon-annealing to achieve interfacial electronic coupling. The hierarchical porosity derived from MOF pyrolysis facilitates rapid mass transport and reactant enrichment; Strong metallic interactions between Co nanoislands and the Cu matrix suppress nanoparticle aggregation while promoting charge redistribution. In addition, the interfacial effect of Cu-Co promotes electron transfer between the two and accelerates the reaction kinetics; Abundant oxygen vacancies (O_V) generated during thermal reduction serve as electron reservoirs, promoting proton-coupled electron transfer during *NHx hydrogenation. Electrochemical evaluations reveal exceptional performance including remarkable NH_3 yield of 57.4±2.9 mg·h^{-1}·mg$_{cat}^{-1}$ and Faraday efficiency of 98.4 ± 1.2% at -1.0 V vs.RHE, outperforming state-of-the-art Cu-based catalysts. In addition, this is also demonstrated by the catalyst C/Cu@Co_3O_4 has excellent durability maintaining its activity over 10 consecutive cycles and more than 100 hours of continuous operation with less than 5% performance loss. This work underscores the potential of interfacial-engineering of electrocatalysts through precise spatial and electronic structure control, paving the way for sustainable nitrate treatment and decentralized ammonia synthesis.

The synthesis pathway of C/Cu@Co_3O_4 catalysts is illustrated in **Fig. 1A.** The process began with a controlled modification of the Cu-BTC

[a] *School of Environmental and Chemical Engineering, Jiangsu University of Science and Technology, Zhenjiang 212003, Jiangsu, PR China.*
[b] *Department of Chemical Engineering, Swansea University, Swansea, SA1 8EN, UK.*
[1] *These authors equally contribute to this work.*
**Corresponding author: fuyang@just.edu.cn; ypzhang@just.edu.cn; mengnan.wang@swansea.ac.uk*

frameworks using a polydopamine (PDA)-mediated cobalt precursor construction. This step enabled the uniform deposition of cobalt species on the MOF surface. Subsequent thermal annealing under argon (500 °C, 2 h) induced structural evolution, resulting in the formation of Co_3O_4-Cu heterostructures with well-defined interfacial features. As evidenced by SEM (**Fig. S1**), pristine Cu-BTC exhibits well-defined octahedral morphology. After PDA-assisted cobalt loading, the intermediate Cu-BTC@Co retained this structure while displaying distinct cobalt nano-islands anchored on the framework surface, indicating successful phase-segregated growth. Upon annealing, the unmodified C/Cu precursor collapsed into irregular aggregates (**Fig. S2A**), whereas the PDA/Co-modified sample preserved approximately 85% of its octahedral shape (**Fig. 1B, S2B**), suggesting that the PDA–Co coating stabilized the structure. Bright spots corresponding to decomposed Cu were also observed within the carbon matrix. TEM analysis (**Fig. 1C**) confirms the Cu substrate was surrounded by the possible Co_3O_4 nanoislands, which forming the hierarchical core@shell architecture. This spatial configuration increases the exposure of active cobalt species and facilitates efficient interfacial electronic interaction. High-resolution TEM (HRTEM) (**Fig. 1D**) and corresponding fast Fourier transform (FFT) (**Fig. 1E-F**) pattern revealed lattice spacings of 0.24 nm and 0.29 nm, corresponding to Co_3O_4 (311) and (220) planes (JCPDS 42-1467), respectively, further verifying the cubic spinel structure of Co_3O_4. In addition, multiple well-defined interfaces were observed where the Co_3O_4 nano-islands are directly attached to the Cu substrate, exhibiting clear lattice continuity across the junctions. This structural coherence indicates strong electronic coupling at the interface, which is expected to facilitate efficient charge transfer during electrocatalysis. Elemental mapping (**Fig. 1G**) results demonstrate uniform Cu distribution along with spatially correlated Co-O signals, confirming the formation core@shell structures with Cu as core and Co_3O_4/C as shell.

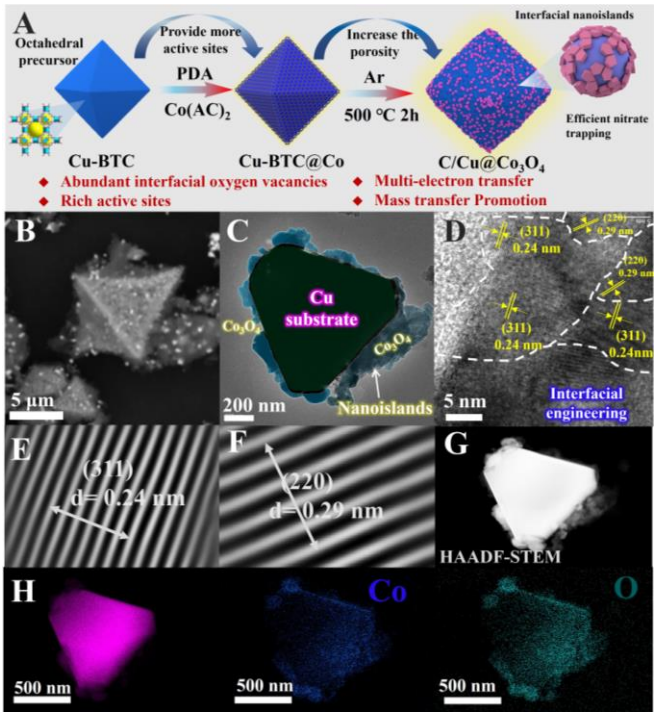

Fig. 1 (A) Schematic representation of the synthesis of C/Cu@Co_3O_4. (B) Scanning electron micrographs of catalyst C/Cu@Co_3O_4. (C) transmission electron mirror (TEM) images. (D) high-resolution TEM images. (E, F) Local magnification of high-resolution TEM. (G) HADDF-STEM image and (H) element mapping images of catalyst C/Cu@Co_3O_4.

The structural properties such as specific surface area and pore size of the catalyst were further evaluated. As shown in **Fig. S3**, the catalysts are featured with mainly microporous structure (1 ~ 2 nm), and the high adsorption capacity of C/Cu@Co_3O_4 in the low-pressure and high pressure indicates a high specific surface area and microporous/ stacked mesoporous structures compared to other derivative counterparts, which is conducive to mass transfer of reactants and exposure of active species. **Fig. 2** presents the structural and surface characterization of the C/Cu@Co_3O_4 catalyst using X-ray diffraction (XRD) pattern and X-ray photoelectron spectroscopy (XPS). **Fig. S4** evidences the initial Cu-BTC metal-organic-framework precursor and PDA modified Cu-BTC derived products. In contrast, the XRD pattern (**Fig. 2A**) confirms the presence of the (111) diffraction peak of metallic Cu substrate in the C/Cu@Co_3O_4 and C/Cu, consistent with the standard card of Cu (PDF#04-0836), indicating that C/Cu@Co_3O_4 affords dominant the crystal structure metallic Cu substrate from the Cu-BTC graphitization process. In addition, no visible Co characteristic diffraction in the XRD pattern can be identified, indicating the low crystallinity and low loading state. Besides, C/Cu@Co_3O_4 showcases negligible diffraction variation compared to Cu-BTC derived C/Cu catalyst, indicating the Co should exist onto the Cu substrate rather than enter into the lattice of metallic Cu phase, further confirming the special configuration of catalyst

XPS analysis further revealed the surface chemical state and elemental environment of C/Cu@Co_3O_4. The dominant elemental composition of Cu, Co, C, N, and O can be identified, demonstrating the special composition of catalyst (**Fig. 2B**). As a note, the Co modified catalyst C/Cu@Co_3O_4 afforded a higher presence of oxygen element and limited exposure of Cu. This mainly attribute to that the existing Co oxides onto the Cu substrate contribute to the increasing oxygen loading and reduce the exposed surface of Cu particles[22, 23]. The XPS spectrum of C 1s (**Fig. 2C**) indicate that all the samples afford the peaks of binding energy at ~284.8 eV and ~288.3 eV corresponding to the C-C and C=O/N moieties, respectively, illustrating the existing carbon framework derived from Cu-BTC precursor. The porous structure of the carbon skeleton significantly increases the specific surface area of the catalyst, triggering rapid mass transfer and diffusion of reactants. The XPS spectrum of Cu 2p (**Fig. 2D, Fig. S5**) showed that Cu^{2+} accounted for 76.3% of the total Cu species in C/Cu@Co_3O_4, significantly higher than that of the catalyst C/Cu and Co-free C/Cu@C. In addition, the electron-deficient Cu^{2+} of C/Cu@Co_3O_4 compared to C/Cu catalyst possibly further promote the multi-electron transfer process between Cu sites and nitrate adsorbed[24, 25]. This would trigger the nitrate activation and later conversion. In particular, the metallic Cu substrate could act as the electron shuttle tunnel, which accelerates the electron transfer.

The Co 2p spectrum of C/Cu@Co_3O_4 (**Fig. 2E**) evidenced the abundant Co^{3+}/Co^{2+} cycles, which benefits to the reaction redox of nitrate reduction. This also indicated the oxidative state of Co species

onto the Cu substrate. The O 1s spectrum (**Fig. 2F, Fig. S6**) exhibited that C/Cu@Co_3O_4 has a higher oxygen vacancy ratio than C/Cu catalyst, indicating that it has a higher active surface[26, 27], further implying a more catalytically active surface. The XPS spectrum of catalyst N 1s (**Fig. S7**) with binding energy at 398.79 eV and 400.3 eV corresponding to pyridine nitrogen and pyrrole nitrogen, respectively, which would facilitate the surface enrichment of nitrate ions during the reaction, enhancing the local reaction concentration and improving nitrate conversion. Taken together, these characterization results demonstrate that the C/Cu@Co_3O_4 catalyst retained the crystal features of its Cu-BTC precursor while the Co coating and PDA-derived carbon layer significantly modified the surface electronic structure, introducing defects and dopants that are favourable for enhanced electrocatalytic nitrate reduction.

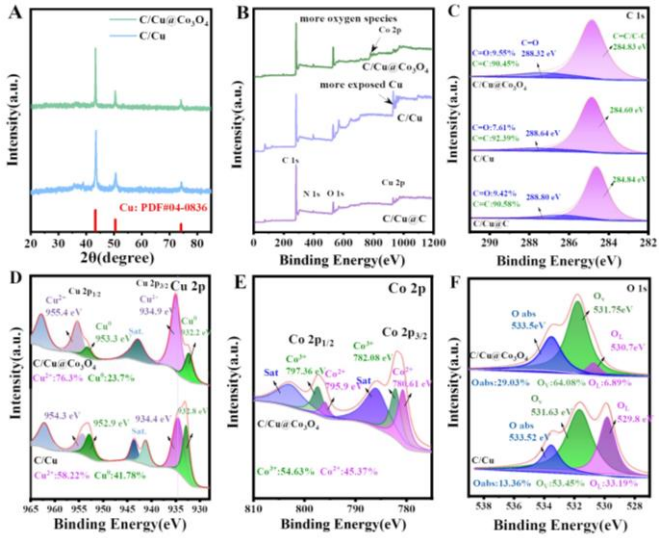

Fig. 2 (A) XRD patterns of catalysts C/Cu@Co_3O_4 and C/Cu. X-ray photoelectron spectroscopy (XPS) spectra of catalysts: full survey (B), C1s core (C), Cu 2p core level (D) of C/Cu@Co_3O_4 and C/Cu; Co 2p core level (E) of C/Cu@Co_3O_4; O 1s core level (F) of C/Cu@Co_3O_4 and C/Cu.

The electrocatalytic performance of C/Cu@Co_3O_4, Cu-BTC, C/Cu, and C/Cu@C catalysts for nitrate reduction (NO_3^-RR) was evaluated in a three-electrode system with a Nafion 117 membrane. Linear sweep voltammetry (LSV) in 0.1 M K_2SO_4 (with/without 0.1 M KNO_3) revealed enhanced current densities in nitrate-containing electrolytes (**Fig. S8**), confirming NO_3^-RR activity when employing the catalyst. Among them, the current density at the same potential follows the order C/Cu@Co_3O_4 > Cu-BTC > C/Cu@C > C/Cu (**Fig. 3D**), preliminarily confirming the superior catalytic activity of C/Cu@Co_3O_4. Within the applied voltage range, the current density dropped most significantly around -1.0 V vs.RHE. Chronoamperometry tests at -0.8 to -1.2 V vs. RHE using C/Cu@Co_3O_4-coated carbon cloth (4 mg·cm^{-3}) in 0.1 M KNO_3/K_2SO_4 showed that the current density remained relatively stable during the reaction (**Fig. 3A**), indicating good operational stability of C/Cu@Co_3O_4 across a wide potential range. UV-vis analysis of the catholyte (**Fig. 3B**) and calibration with an NH_3 standard curve (**Fig. S9**) quantified the NH_3 yield (57.4 ± 2.9 mg·h^{-1}·mg$_{cat}^{-1}$) and FE (98.4 ± 1.2%) at -1.0 V vs. RHE (**Fig. 3C**). Compared with the catalyst C/Cu@C, C/Cu@Co_3O_4 has about 2.2 times the NH_3 yield and 1.3 times the FE, significantly outperforming all counterparts (**Fig. 3F**). C/Cu and C/Cu@C followed a similar trend (**Fig. S12–S14**), but their NH_3 yields and efficiencies were significantly lower, highlighting the role of Co coating in enhancing activity and selectivity. According to EIS analysis, the reason for the enhancement of C/Cu@Co_3O_4 activity is its low charge transfer resistance (**Fig. 3E**), attributed to the efficient electron transport pathway provided by the metallic Cu core and Co_3O_4 nanoislands[28]. Compared with other catalysts, it has obvious advantages. **Fig. S15** and Supplementary **Table. S1** compare the electrocatalytic NO_3^-RR performances of C/Cu@Co_3O_4 with other extensively reported electrocatalysts, and to our best knowledge, the NH_3 Yield and FE of C/Cu@Co_3O_4 outperform most reported results. In addition, compared with Cu_5Co_5 catalysts[29], they have similar elemental compositions, but the electrocatalytic performance of C/Cu@Co_3O_4 has been greatly improved, indicating that Co_3O_4 interface engineering can promote electrocatalytic nitrate reduction. The long-term stability tests over 10 cycles and 100 hours of operation demonstrated less than 5% activity decay, underscoring its practical viability (**Fig. 3H-I**). In addition, the XRD and XPS results (**Fig. S16**) of the used catalyst after the reaction confirm the reservation of structure of catalyst, further proving its long-term stability. To monitor product accumulation during extended use, the electrolyte was sampled at multiple time points (1–12 h) without replacement. Using standard curve (**Fig. S9~S11**), concentrations of NO_3^-, NO_2^-, and NH_4^+ were quantified (**Fig. S17**) and key metrics including nitrate removal, residual NO_3^-, NO_2^- selectivity, and NH_4^+ selectivity were calculated for all catalysts (**Fig. 3G**). C/Cu@Co_3O_4 achieved a nitrate conversion rate of 60.42% after 12 hours, with minimal NO_2^- accumulation (3.09 ppm), indicating high selectivity towards NH_3. In summary, the C/Cu@Co_3O_4 catalyst demonstrates excellent electrocatalytic activity and long-term stability for the nitrate reduction reaction, establishing its promise for efficient and durable NH_3 production.

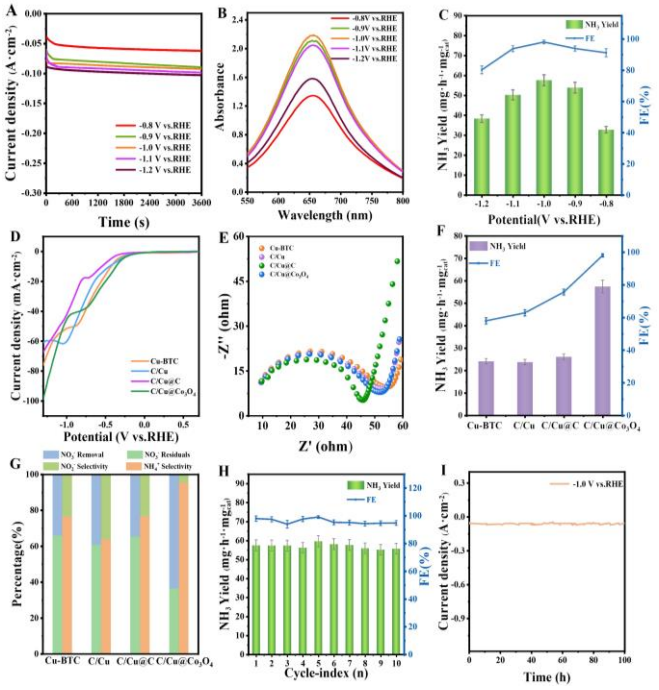

Fig. 3 (A) I-T curves of catalyst C/Cu@Co_3O_4 at different voltages. (B) UV-vis spectra of electrolyte in the cathode chamber stained with iodophil indicator. (C) NH_3 yield and Faradaic efficiency of catalyst C/Cu@Co_3O_4 at different potentials. (D) LSV curves of catalysts C/Cu@Co_3O_4, Cu-BTC, C/Cu and C/Cu@C samples in 1M K_2SO_4 solution with NO_3^-. (E) Electrochemical impedance spectrum (EIS) of catalysts Cu-BTC, C/Cu, C/Cu@C, C/Cu@Co_3O_4. (F) comparison of NH_3 yield and Faraday efficiency of different catalysts at -1.0 V vs. RHE. (G) Normalized plots of NO_3^- removal, NO_3^- residuals, NO_2^- selectivity, and NH_4^+ selectivity for all catalysts reacted for 12 h; (H) Continuous cycling tests of catalyst C/Cu@Co_3O_4 at -1.0 V vs.RHE; (I) I-T tests of catalyst C/Cu@Co_3O_4 in continuous electrolysis for 100 h at -1.0 V vs.RHE.

To further clarify the nitrogen source in the nitrate reduction reaction (NO_3^-RR), K_2SO_4 and KNO_3 were used as electrolytes respectively in this study, and 1hour electrolysis experiments were conducted at -1.0V vs.RHE potential. As shown in the UV–vis spectra (**Fig. S18A**), the absorption intensity in the K_2SO_4 system was significantly lower than that of the KNO_3 system, and close to the baseline, indicating that no NH_3 was generated when nitrate was absent. Similarly, low absorbance was observed under open-circuit conditions and when carbon cloth without catalyst was used as the working electrode, further ruling out the possibility of ammonia formation from environmental contamination or catalyst impurities. These results confirmed that NH_3 was produced only when both nitrate and the catalyst were present under applied potential, indicating the detected NH_3 originated from the electrocatalytic nitrate reduction process. To further validate the nitrogen source, an isotopic labelling experiment was conducted with ^{15}N-labbeled nitrate, as shown in **Fig. S18C**. When $K^{14}NO_3$ was used as the electrolyte of the reactant, the NMR spectrum showed a characteristic triplet corresponding to $^{14}NH_4^+$. In contrast, replacing the electrolyte with $K^{15}NO_3$, resulted in a distinct doublet peak corresponding to $^{15}NH_4^+$, confirming that the detected nitrate originates from electrocatalytic nitrate reduction. Since the adsorption of nitrate ions on the catalyst surface is a key step to determine its reactivity, we further investigated the adsorption properties of different catalysts in 100 ppm nitrate solution. The experimental results show that (**Fig. S19**) C/Cu@Co_3O_4 catalyst exhibits the most significant UV absorption feature, which confirms that catalyst surface has a higher NO_3^- adsorption capacity. This enhanced adsorption likely facilitates the local enrichment of NO_3^- near the active site of the C/Cu@Co_3O_4 catalyst, thus promoting the efficient generation of NH_3. This observation helps explain the superior catalytic performance of C/Cu@Co_3O_4 in the NO_3^-RR process.

In conclusion, the C/Cu@Co_3O_4 catalyst, featuring spatially confined Co_3O_4 nanoislands on a metallic Cu substrate, achieves exceptional NO_3^- to NH_3 conversion with a yield of 57.4 ± 2.9 $mg \cdot h^{-1} \cdot mg_{cat}^{-1}$ and near-unity FE of 98.4 ± 1.2% at -1.0 V vs.RHE. Its hierarchical structure, featuring carbon framework supporting metallic Cu core and interface-engineered Co_3O_4 nanoislands shell, promotes nitrate adsorption, accelerates electron transfer, and suppresses HER competition, demonstrating long-term stability with over 100 hours of operation and less than 5% activity decay, along with high selectivity evidenced by 60.42% nitrate conversion and only 3.09 ppm nitrite byproduct formation, underscoring its practical viability for sustainable ammonia synthesis.

Data available on request from the authors

Conflicts of interest

There are no conflicts to declare.

Acknowledgement

The research received financial support from the Natural Science Foundation of Jiangsu province (BK20241950).

References

1. W. He, J. Zhang, S. Dieckhöfer, et al, Nat. Commun.. 2022, **13**, 1129.
2. Y. Ashida, K. Arashiba, K. Nakajima, et al, Nature. 2019, **568**, 536-540.
3. X. Zhong, E. Yuan, F. Yang, et al, Proceed. Nat. Acad. Sci. U. S. A. 2023, **120**, e2306673120.
4. H. Li, M. Aizudin, S. Yang, et al, Sep. Purif. Technol. 2023, **326**, 124802.
5. V. Kyriakou, I. Garagounis, A. Vourros, et al, Joule. 2020, **4**, 142-158.
6. Y. Liu, X. Zhong, M. Liu, et al, Appl. Catal. B: Environ. Energy. 2024, **355**, 124205.
7. H. Lu, K.N. Opoku, Z. Wang, et al, Chem. Eng. J. 2025, **503**, 158536.
8. S. Yang, W. Zhang, M. Liu, et al, J. Environ. Chem. Eng. 2023, **11**, 109190.
9. J. Deng, J.A. Iñiguez, C. Liu, Joule. 2018, **2**, 846-856.
10. G. Qing, R. Ghazfar, S.T. Jackowski, et al, Chem. Rev. 2020, **120**, 5437-5516.
11. J. Jiang, Y. Fang, Y. Zhao, et al, Mol. Catal. 2023, **547**, 113313.
12. H. Zhu, Z. Wang, L. Cao, et al, Chem. Commun., 2025, **61**, 7065-7068.
13. Y. He, M. Wang, S. Liu, et al, Chem. Eng. J. 2023, **454**, 140106.
14. Z.-Y. Wu, M. Karamad, X. Yong, et al, Nat Commun. 2021, **12**, 2870.
15. Q. Hu, Y. Qin, X. Wang, et al, Energy Environ. Sci. 2021, **14**, 4989-4997.
16. N. Zhang, H. Sun, M.-y. Wang, et al, Mol. Catal. 2023, **544**, 113187.
17. H. Hirakawa, M. Hashimoto, Y. Shiraishi, et al, ACS Catal. 2017, **7**, 3713-3720.
18. P.H. van Langevelde, I. Katsounaros, M.T.M. Koper, Joule. 2021, **5**, 290-294.
19. P. Liu, J. Yan, H. Huang, et al, Chem. Eng. J. 2023, **466**, 143134.
20. X. Liu, Y. Wang, Z. Hu, et al, Appl. Catal. B: Environ. Energy. 2025, **371**, 125254.
21. J. Sun, X. Zhang, H. Zhang, et al, J. Electroanal. Chem. 2023, **936**, 117377.
22. H. Li, Y. Jiang, X. Li, et al, J. Am. Chem. Soc. 2023, **145**, 14335-14344.
23. F. Zhao, G. Hai, X. Li, et al, Chem. Eng. J. 2023, **461**, 141960.
24. T. Zhu, Q. Chen, P. Liao, et al, Small. 2020, **16**, 2004526.
25. G. Jiang, M. Peng, L. Hu, et al, Chem. Eng. J. 2022, **435**, 134853.
26. H. Lu, K. N. Opoku, Z. Wang, et al, Chem. Eng. J. 2025, **503**, 158536.
27. L. Liu, C. Han, G. Ding, et al, Chem. Eng. J. 2022, **450**, 138302.
28. Z. Cen, Z. Ni, X. Zhou, et al, J. Environ. Chem. Eng. 2023, **11**, 110079.
29. J. Zhao, L. Liu, Y. Yang, et al, ACS Sustain. Chem. Eng. 2023, **11**, 2468-2475.